Nuclear Instruments and Methods in Physics Research B 383 (2016) 52–58

Contents lists available at ScienceDirect

Nuclear Instruments and Methods in Physics Research B

journal homepage: www.elsevier.com/locate/nimb

Bragg-edge neutron transmission strain tomography for *in situ* loadings

C.M. Wensrich [a,*], J.N. Hendriks [a], A. Gregg [a], M.H. Meylan [b], V. Luzin [c], A.S. Tremsin [d]

[a] School of Engineering, The University of Newcastle, Callaghan, NSW 2308, Australia
[b] School of Mathematical and Physical Sciences, The University of Newcastle, Callaghan, NSW 2308, Australia
[c] Bragg Institute, Australian Nuclear Science and Technology Organisation (ANSTO), Kirrawee, NSW 2232, Australia
[d] Space Sciences Laboratory, University of California, Berkeley, CA 94720, USA

ARTICLE INFO

Article history:
Received 6 May 2016
Received in revised form 17 June 2016
Accepted 19 June 2016
Available online 27 June 2016

Keywords:
Strain tomography
Bragg-edge imaging
Neutron diffraction
Neutron transmission strain measurement

ABSTRACT

An approach for tomographic reconstruction of three-dimensional strain distributions from Bragg-edge neutron transmission strain images is outlined and investigated. This algorithm is based on the link between Bragg-edge strain measurements and the Longitudinal Ray Transform, which has been shown to be sensitive only to boundary displacement. By exploiting this observation we provide a method for reconstructing boundary displacement from sets of Bragg-edge strain images. In the case where these displacements are strictly the result of externally applied tractions, corresponding internal strain fields can then be found through traditional linear-static finite element methods. This approach is tested on synthetic data in two-dimensions, where the rate of convergence in the presence of measurement noise and beam attenuation is examined.

1. Bragg-edge strain measurement and the Longitudinal Ray Transform (LRT)

Bragg-edges are a term given to discrete jumps in the relative transmission rate of neutrons through polycrystalline samples as a function of wavelength, λ [1]. These edges are formed through diffraction with their positions related to lattice spacings within the sample through Bragg's law. In simple terms, in a polycrystalline sample neutrons can be coherently scattered by crystal planes of a certain spacing up until their wavelength corresponds to a scattering angle of 180° (i.e. backscattered). This wavelength is given by two times the corresponding lattice '*d*-spacing', and no further (coherent) scattering by this lattice plane occurs above this value. This creates an abrupt increase in the relative transmission rate.

Multiple Bragg-edges can be found from a typical sample corresponding to various lattice spacings within the crystal structure. This can provide a wealth of structural information, or in the case of this paper, minute shifts in the position of edges can be used to measure strain within the sample of the form;

$$\langle \epsilon \rangle = \frac{d - d_0}{d_0}, \tag{1}$$

where $\langle \epsilon \rangle$ is the normal stain in the direction of transmission averaged over the irradiated volume, d is the measured lattice spacing and d_0 is the same spacing in an unstressed sample. Like all diffraction techniques, strain measured in this way refers only to the elastic portion of deformation which is related to stress through Hooke's law (see [2–5]).

While other approaches exist (e.g. [6]), the most common experimental technique for measuring Bragg-edges relies on the use of energy-resolved, or 'time-of-flight', neutron detectors at pulsed neutron sources [1,3]. This technology has undergone significant development with pixelated detectors being in existence for more than 10 years [7]. The current generation of detectors consist of an array of up to 512 × 512 pixels with spatial resolution of 55 μm and temporal resolution of 100 ps[1]; each one capable of simultaneously measuring a transmission spectra [8]. This has allowed the possibility of high resolution strain imaging, where two dimensional projections of the strain field within a sample can be made in an analogous way to a traditional radiograph [9].

From the outset, the first demonstration of strain imaging raised the tantalising prospect of tomographic reconstruction of three-dimensional strain fields. As opposed to conventional tomographic imaging of scalar fields (e.g. X-ray CT and MRI), the problem here is the reconstruction of tensor fields – a significantly

* Corresponding author.
E-mail address: christopher.wensrich@newcastle.edu.au (C.M. Wensrich).

[1] The corresponding energy/wavelength resolution depends on the length of the instrument. For example, with a flight tube 40 m in length, 100 ps corresponds to a wavelength resolution of around 10^{-8} Å.

http://dx.doi.org/10.1016/j.nimb.2016.06.012
0168-583X/

more complex problem. Initial work in this area focused on the special case of axisymmetric systems (e.g. [10–12]), however it was recently shown by Lionheart and Withers [13] that a general solution to the reconstruction problem is not possible. An overview of this argument is as follows:

Say we have a body, B, subject to a displacement field $\boldsymbol{\phi}(\boldsymbol{x})$ as shown in Fig. 1. In the absence of attenuation effects and assuming a ray of infinitesimal cross section, a single strain measurement from a given pixel in an energy-resolved detector can be expressed as;

$$\langle \epsilon \rangle = I_\epsilon(\boldsymbol{x_0}, \hat{\boldsymbol{n}}) = \frac{1}{L}\int_0^L \epsilon_{ij}(\boldsymbol{x_0} + s\hat{\boldsymbol{n}})\hat{n}_i\hat{n}_j ds, \tag{2}$$

where the corresponding ray in the direction $\hat{\boldsymbol{n}}$ enters B at the point $\boldsymbol{x_0} \in \partial B$ and exits at $\boldsymbol{x_0} + L\hat{\boldsymbol{n}} \in \partial B$, with internal strain defined as $\epsilon_{ij} = \frac{1}{2}(\phi_{i,j} + \phi_{j,i})$.[2] I_ϵ is a form of ray transform, specifically known as the Longitudinal Ray Transform (LRT) [13].

Along the ray, we can write $\frac{d\phi_i}{ds} = \phi_{i,j}\frac{dx_j}{ds} = \phi_{i,j}n_j$, and (2) becomes;

$$I_\epsilon(\boldsymbol{x_0}, \hat{\boldsymbol{n}}) = \frac{1}{L}\int_0^L \frac{1}{2}(d\phi_i\hat{n}_i + d\phi_j\hat{n}_j) = \frac{1}{L}(\phi_i(\boldsymbol{x_0} + L\hat{\boldsymbol{n}}) - \phi_i(\boldsymbol{x_0}))\hat{n}_i \tag{3}$$

This result indicates that I_ϵ is only sensitive to displacement of the boundary of B. Given that multiple strain fields exist that result in no boundary deformation, it implies that the LRT has a non-trivial kernel and therefore has no inverse. For a simple example; consider the case of a uniform two-dimensional plate that is fully constrained at its perimeter. Under the action of a body force such as gravity, the strain field within this plate would be non-zero; however, in terms of the LRT, this would be indistinguishable from the undeformed case ($I_\epsilon = 0$ in both cases).

As was pointed out by Lionheart and Withers [13], this presents a serious problem in terms of general tomographic reconstruction of strain; a given boundary deformation does not uniquely define the strain field within an object.

2. Tomography via boundary displacement reconstruction

While the argument from Lionheart and Withers is true in a general sense, there are often physical realities that do lead to a trivial kernel. For example, if a uniform elastic body is only subject to boundary tractions (i.e an *in situ* loading in the absence of all body forces and eigenstrains [14]), then there is an obvious (injective) link between the internal strain field and boundary deformation; an absence of boundary deformation obviously implies zero strain in this case.

This observation provides a potential approach to tomographic reconstruction of strain for this class of problems. This strategy is as follows;

1. Utilising Eq. (3), reconstruct the elastic component of displacement over the entire boundary of the object.
2. Calculate the internal strain field by solving the resulting Dirichlet boundary value problem.

A numerical implementation of this approach (adapted from [15]) is as follows;

2.1. Numerical algorithm

In the first stage, we are concerned with the reconstruction of boundary deformation. To this end, we begin by discretising the surface of the body using a triangular mesh with n_v vertices (or 'nodes') with $3n_v$ unknown Cartesian displacements. A given ray can enter and leave the body at arbitrary points; the displacement of which can be related back to the nodes through interpolation via linear shape functions.

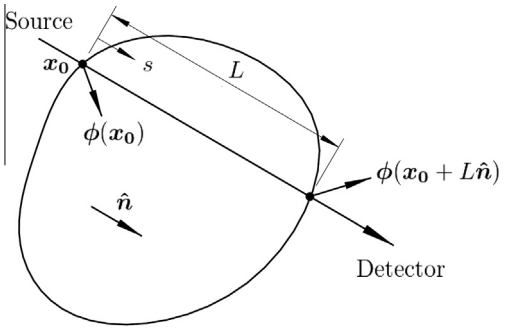

Fig. 1. Strain within a body measured by an idealised ray in a Bragg-edge time-of-flight transmission neutron experiment. This measurement represents the normal component of strain in the direction $\hat{\boldsymbol{n}}$, averaged along the path. It can be expressed as the relative change of the length of the path through the body.

Say a ray intersects a given mesh element at $\boldsymbol{x}$ as shown in Fig. 2. With reference to the displacement of the three corresponding nodes, $\boldsymbol{\phi}_1, \boldsymbol{\phi}_2$, and $\boldsymbol{\phi}_3$, we can approximate the displacement at $\boldsymbol{x}$ using linear shape functions as;

$$\boldsymbol{\phi}(\boldsymbol{x}) = \lambda_1\boldsymbol{\phi}_1 + \lambda_2\boldsymbol{\phi}_2 + \lambda_3\boldsymbol{\phi}_3, \tag{4}$$

where $\lambda_i = \frac{A_i}{A}$ for $i \in \{1,2,3\}$ and $A = \sum A_i$ is the total area of the element.

Through Eq. (3), we can now express the strain measured by a given Bragg-edge measurement in matrix form as;

$$\begin{aligned}\langle \epsilon \rangle = I_\epsilon(\boldsymbol{x}^p, \hat{\boldsymbol{n}}) &= \frac{1}{L}\begin{bmatrix}\hat{\boldsymbol{n}}^T & -\hat{\boldsymbol{n}}^T\end{bmatrix}\begin{bmatrix}\boldsymbol{\phi}^q \\ \boldsymbol{\phi}^p\end{bmatrix} \\ &= \frac{1}{L}\left(\begin{bmatrix}\hat{\boldsymbol{n}}^T\lambda_1^q & \hat{\boldsymbol{n}}^T\lambda_2^q & \hat{\boldsymbol{n}}^T\lambda_3^q\end{bmatrix}\begin{bmatrix}\boldsymbol{\phi}_1^q \\ \boldsymbol{\phi}_2^q \\ \boldsymbol{\phi}_3^q\end{bmatrix} - \begin{bmatrix}\hat{\boldsymbol{n}}^T\lambda_1^p & \hat{\boldsymbol{n}}^T\lambda_2^p & \hat{\boldsymbol{n}}^T\lambda_3^p\end{bmatrix}\begin{bmatrix}\boldsymbol{\phi}_1^p \\ \boldsymbol{\phi}_2^p \\ \boldsymbol{\phi}_3^p\end{bmatrix}\right),\end{aligned} \tag{5}$$

where superscript p refers to the entry point, q refers to the exit and $L = \|\boldsymbol{x}^q - \boldsymbol{x}^p\|$.

Note that this calculation has been split into two parts corresponding to the entry and exit. In principal these could be combined into one matrix, however if the mesh elements are neighbours it is possible for some of the vertices to be repeated. It should also be noted that this expression is constructed for a convex body, however it could be trivially extended to a non-convex body by considering differences between each instance of an entry and exit of the ray.

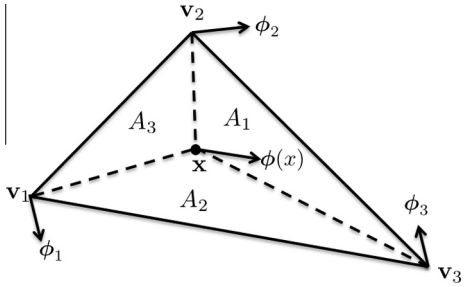

Fig. 2. Interpolation of displacement at a point $\boldsymbol{x}$ within a triangular mesh element on the surface of a body. The areas of the sub triangles are denoted by A_1, A_2, and A_3. The nodal displacements are given by $\boldsymbol{\phi}_1, \boldsymbol{\phi}_2$, and $\boldsymbol{\phi}_3$. The displacement at the point $\boldsymbol{x}$ is $\boldsymbol{\phi}(\boldsymbol{x})$.

[2] It is easily shown that $I_\epsilon(\boldsymbol{x_0}, \hat{\boldsymbol{n}}) = I_\epsilon(\boldsymbol{x_0} + \zeta\hat{\boldsymbol{n}}, \hat{\boldsymbol{n}}), \forall \zeta \in \mathbb{R}$ where integration limits are adjusted to suit.